



# Structural, optical and dielectric characterization of Au/HfO<sub>2</sub>/(Pt,TiN) capacitors



F. El Kamel<sup>a,\*</sup>, Z. Ben Cheikh<sup>a</sup>, M.A. Soussou<sup>b</sup>, A. Moadhen<sup>c</sup>, K. Khirouni<sup>a</sup>

<sup>a</sup> LaPhyMNE, University of Gabes, 6072, Tunisia

<sup>b</sup> Thermal Processes Laboratory (CERT), Hammam Lif 2050, Tunisia

<sup>c</sup> Unité de Recherche en Nanomatériaux et Photonique, University of Tunis El Manar, 2092, Tunisia

## ARTICLE INFO

### Keywords:

Electrical measurements  
HfO<sub>2</sub> films  
Oxygen vacancies  
Structural and optical properties

## ABSTRACT

Structural, optical and dielectric properties of atomic layer deposited HfO<sub>2</sub> were studied in close relation with the bottom electrode nature. We used XRD, HRTEM and AFM to study the internal microstructure and the surface roughness of the films. The HfO<sub>2</sub>/Pt sample shows a mixture of monoclinic and orthorhombic phases whereas the HfO<sub>2</sub>/TiN sample presents few crystallites in orthorhombic structure dispersed in a badly crystallized or amorphous phase. Raman spectroscopy shows that between 100 and 800 cm<sup>-1</sup>, the HfO<sub>2</sub>/Pt device displays 13 Raman-active modes whereas the HfO<sub>2</sub>/TiN device reveals 10 Raman-active modes. Using the UV–Vis reflectance spectra, we expect both direct and indirect electronic transitions with optical band-gap energies of 5.11 and 4.61 eV, respectively. Photoluminescence spectroscopy allows the identification of localized states in the HfO<sub>2</sub> band-gap. PL emission spectra consist of five sub-peaks, centered at around 1.64–1.92 eV, 2.10 eV and 2.33 eV. These energies are close to the trap levels calculated for oxygen vacancies, involved during the film deposition. As the temperature is increased up to 380 °C, an obvious dispersion of the real permittivity takes place in the low frequency domain. This behavior, highly enhanced by the oxygen vacancies mobility, is typical for the electrode polarization process.

## 1. Introduction

High- $\kappa$  oxides [1–6] with high capacitance value, good voltage linearity and low leakage currents are emerging in the microelectronic industry. Among these oxides, HfO<sub>2</sub> is being intensively investigated for its prospective application as storage medium for non-volatile resistive random access memories (RRAMs) [6] and as dielectric oxide for metal-oxide-semiconductor field-effect transistor (MOSFET) stacks [7] and metal-oxide-metal (MOM) capacitors [8]. However, HfO<sub>2</sub> provides a significant density of oxygen vacancies [9], which has remarkable influence on its properties. Thus, it is necessary to understand the “defect/property” relationship.

Moreover, several authors [10] have reported an influence of the oxide/metal interface on the electrical properties of the capacitor devices. They showed that better reliability and performances are usually obtained with noble metals (such as Au or Pt) than with highly oxidizable electrodes (such as TiN or Ti), albeit they are not convenient for microelectronic industry. Actually, TiN has a strong affinity to the oxygen atoms, resulting in oxygen depletion in the oxide bulk and oxidized TiN at the interface. This feature alters the cycling properties

of the RRAMs [11] by developing stronger filaments that are hard to disrupt in the reset step. As well, the oxidized layer at the oxide/TiN interface could be responsible for the linearity degradation in the MOM structures [12].

Although numerous recent reports were done on the electrical behavior of M/HfO<sub>2</sub>/M capacitors, there is a lack of information on their optical and structural characterization in close relation with the dielectric properties. This will constitute the main purpose of the present work, where two different bottom metal electrodes (Pt and TiN) were used.

## 2. Experimental details

HfO<sub>2</sub> films were grown by atomic layer deposition (ALD) on both Pt/Ti/Si and TiN/Pt/Ti/Si substrates using alternating pulses of hafnium tetrachloride (HfCl<sub>4</sub>) and purified H<sub>2</sub>O with N<sub>2</sub> as a carrier gas. The ALD process was performed in an ASM Pulsar® 2000 module (with a growth rate of 0.1 nm/cycle) within the thermal budget of CMOS back end of line (350 °C) at a chamber pressure of 1 Torr. No post-deposition treatment was realized.

\* Corresponding author.

E-mail address: [fadhel.kamel@fsg.rnu.tn](mailto:fadhel.kamel@fsg.rnu.tn) (F. El Kamel).

The crystalline phase identification was carried out by room temperature X-ray diffraction (XRD) analyses in a Bruker® AXS-D5000 diffractometer (Bragg-Brentano  $\theta/2\theta$  geometry), using Cu-K $\alpha$  ( $\lambda = 0.15418$  nm) radiation. The microstructure of cross-sectional samples was analyzed using a FEI Tecnai® G<sup>2</sup> high resolution transmission electron microscope (HR-TEM) operating at 200 kV with a LaB<sub>6</sub> filament. Samples were prepared by tripod polishing and imaged in the [110] orientation. Local chemical analysis was performed using the energy dispersive X-ray spectroscopy (EDS).

Jobin Yvon® (model: T64000) Raman system was used for both Raman and photoluminescence (PL) measurements. A 488 nm (2.54 eV) line from an argon ion laser was used as an excitation source to illuminate the samples with 1  $\mu$ m spot size, keeping its maximum output optical power at  $\sim$ 5 mW. UV–Vis spectra were taken using a Shimadzu® (UV-3101 PC) UV–Vis–NIR scanning spectrophotometer in a diffuse reflection mode to determine the band-gap energy of the HfO<sub>2</sub> films. Background measurements with bare substrates have been performed at first to subtract their contribution. All optical analyses were performed at room temperature.

Top Au-electrodes were deposited by thermal evaporation through a shadow mask to constitute planar MIM capacitors of 1.77 mm<sup>2</sup> area. The dielectric measurements were carried out on these capacitors as a function of temperature using a Novocontrol® impedance analyzer. The temperature control was performed using a Linkam® hot-stage. During the dielectric measurements, samples were enclosed in a dark shielded cell filled with dry nitrogen gas.

### 3. Results and discussion

Fig. 1 displays the XRD patterns for 10 nm-HfO<sub>2</sub>/Pt/Si, 10 nm-HfO<sub>2</sub>/TiN/Si and 20 nm-HfO<sub>2</sub>/TiN/Si films.

Triyoso et al. [13] evidenced that the large scale crystallization of HfO<sub>2</sub> films occurs at around 350 °C, below this temperature they remain amorphous. On Pt substrate, the XRD patterns denote the reflection peaks of (111) at 28.45° (preferential growth direction) and (111) at 31.67° for the HfO<sub>2</sub> monoclinic lattices and a reflection peak of (111) at 30.40° for the HfO<sub>2</sub> orthorhombic lattices. A mixture of monoclinic and orthorhombic phases in atomic layer deposited HfO<sub>2</sub> films was previously reported by Ritala [14] and Cheynet [15]. In addition, Jorel

et al. [16] studied the attenuated total reflectance (ATR) spectra of HfO<sub>2</sub> with different thicknesses and stated that the 11 nm-thick film has a less monoclinic signature than thinner films (< 7 nm). They attributed this feature to the possible growth of an additional orthorhombic phase. The average crystallites size  $s_{(hkl)}$  was estimated based on the Scherer's semi-empirical expression:

$$s_{hkl} = \frac{k \times \lambda_{X-ray}}{\beta_{hkl} \times \cos \theta_{hkl}} \quad (1)$$

where,  $k$  is the shape factor usually taken as equal to 0.9 and  $\lambda_{X-ray} = 0.15418$  nm is the X-ray radiation wavelength.  $\theta_{hkl}$  (in degrees) and  $\beta_{hkl}$  (in radians) are respectively the Bragg angle and the full width at half maximum (FWHM) of the main diffraction peak, determined by fitting this XRD peak to a Lorentzian line shape (see inset of Fig. 1). We used the m-HfO<sub>2</sub> (111) peak, well-developed at  $2\theta = 28.45^\circ$ , to calculate an average crystallites mean size of about 9.8 nm.

On TiN substrate, the XRD patterns show primarily a broad shoulder characteristic of an amorphous phase, with a very weak diffraction peak at 30.40° which corresponds to a small crystalline fraction in the (111) orthorhombic phase. The 10 nm thick HfO<sub>2</sub> film presents only few crystalline domains that are dispersed in a badly crystallized or amorphous matrix (so, the crystallinity could not be detected) whereas the XRD pattern recorded on the 20 nm thick HfO<sub>2</sub> film shows an increase of nm-size crystallites. Actually, thicker films are known to facilitate the crystal nucleation [14], so it is not surprising that the crystallization of HfO<sub>2</sub> films on TiN substrate begins to be clearly observed by XRD for the 20 nm thick films. We presume that in the beginning of the film deposition, TiN can scavenge more oxygen from the HfO<sub>2</sub> than Pt metal electrode, which induce more and more oxygen vacancies at the HfO<sub>2</sub>/TiN interface. Accordingly, the film crystallinity decreases due to the oxygen deficient lattices. Similar behavior was recently observed by Calka et al. [17] on the HfO<sub>2</sub>/Ti interface. Moreover, Jorel et al. [16] performed physical and optical analyses to characterize the chemical bonding states at the HfO<sub>2</sub>/TiN interface. They found an indication of oxygen depleted HfO<sub>2</sub> on the TiN substrate and identified both TiN<sub>x</sub>O<sub>y</sub> and TiO<sub>z</sub> phases with a thickness of 1.5–2 nm.

The other XRD peaks were attributed to the (111) reflection of cubic Pt at 39.78°, (200) reflection of cubic TiN at 42.58°, (111) and (200) reflections of cubic Au at 38.27° and 44.50°, respectively. Finally, peaks appearing at 33.00°, 34.47° and 35.88° were attributed to the multiple reflections of Si, K $\beta$  radiation of Au and K $\beta$  radiation of Pt, respectively. All reflections were indexed using the powder diffraction ICDD card files; Pattern: 00-034-0104 for m-HfO<sub>2</sub>, Pattern: 01-070-2832 for o-HfO<sub>2</sub>, Pattern: 00-004-0802 for fcc-Pt, Pattern: 00-038-1420 for fcc-TiN, Pattern: 00-004-0784 for fcc-Au.

Cross-section HRTEM analyses were performed on the 10 nm-HfO<sub>2</sub>/Pt structure. The image displayed in Fig. 2a is selected out of many. The HfO<sub>2</sub> film shows a constant thickness and sharp interface with Pt. Conversely, the HfO<sub>2</sub>/TiN interface was reported to be more diffuse, maybe due to the growth of TiN<sub>x</sub>O<sub>y</sub> parasitic layer [18]. A typical polycrystalline microstructure, predominantly in monoclinic phase, is obviously identified in the HfO<sub>2</sub>/Pt structure with grains width of few tens of nanometers. Few zones composed of randomly oriented grains, probably in orthorhombic structure according to the XRD data, can also be observed. A zoom (Fig. 2b) is superimposed to Fig. 2a in order to show up one nanocrystallite.

The fast Fourier transform (Fig. 2c) allows to clearly distinguishing between monoclinic and orthorhombic structures and agrees with a mixture of both phases. Moreover, Moiré fringes can be distinguished as a result of the lattices interference. This feature confirms the nanocrystalline structure of the HfO<sub>2</sub> film in all the directions. The most frequent inter-plane distances  $d_{hkl}$ , measured in HfO<sub>2</sub> real space, according to the HRTEM images, are 3.15 and 2.90 Å. These distances could be attributed to the (111) and (111) inter-plane spacings of monoclinic and orthorhombic phases, respectively. Large grain

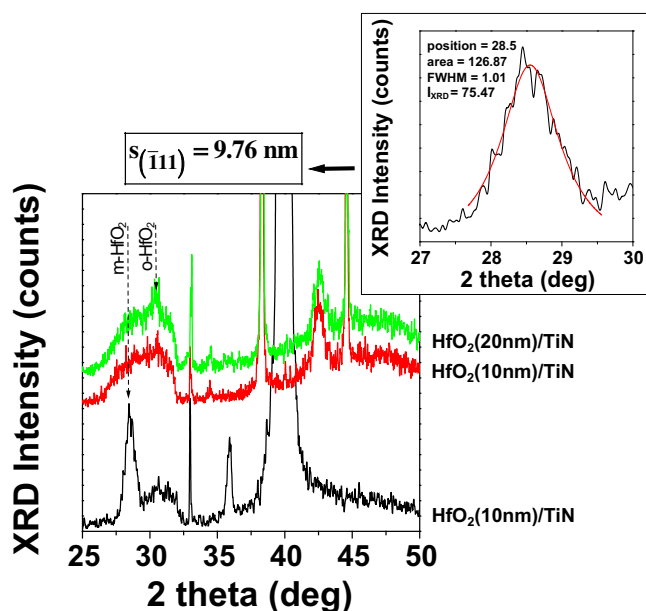


Fig. 1. XRD patterns of 10 nm-HfO<sub>2</sub>/Pt/Si, 10 nm-HfO<sub>2</sub>/TiN/Si and 20 nm-HfO<sub>2</sub>/TiN/Si structures using Cu-K $\alpha$  radiation. The inset displays a zoom of the m-HfO<sub>2</sub> (111) peak, well-developed at 28.45°.

Download English Version:

<https://daneshyari.com/en/article/8033255>

Download Persian Version:

<https://daneshyari.com/article/8033255>

[Daneshyari.com](https://daneshyari.com)